CHAPTER 2

EXPERIMENTAL TECHNIQUES

CHAPTER 2

EXPERIMENTAL TECHNIQUES

2.1 Overview

This chapter deals with experimental methods and characterization techniques utilized in the thesis. This chapter explains sample preparation, fabrication methods, characterization techniques, and their working principles in detail.

This chapter consists of three sections:

(a) Different synthesis and materials fabrication techniques are involved in sample preparation.

(b) Characterization techniques used for crystal structure analysis, magnetic and ferroelectric analysis.

(c) Data analysis tools such as X-ray Rietveld refinement, microstructural study, MPMS, and impedance spectroscopy.

2.2 Synthesis Technique

For the synthesis of all the systems, mainly two different synthesis routes were employed here. The schematic representation of the two routes is explained below:

2.2.1 Sol-Gel synthesis

In materials science, the sol–gel process is a method for producing solid materials from small molecules. The method is used for the fabrication of metal oxides. The process involves the conversion of monomers into a colloidal solution (*sol*) that acts as the precursor for an integrated network (or *gel*) of either discrete

particles or network polymers. Typical precursors are metal alkoxides. Sol-gel process is used to produce ceramic nanoparticles. In this chemical procedure, a "sol" (a colloidal solution) is formed that then gradually evolves towards the formation of a gel-like diphasic system containing both a liquid phase and solid phase whose morphologies range from discrete particles to continuous polymer networks. In the case of the colloid, the volume fraction of particles (or particle density) may be so low that a significant amount of fluid may need to be removed initially for the gel-like properties to be recognized. This can be accomplished in any number of ways. The simplest method is to allow time for sedimentation to occur, and then pour off the remaining liquid. Centrifugation can also be used to accelerate the process of phase separation.

Removal of the remaining liquid (solvent) phase requires a drying process, which is typically accompanied by a significant amount of shrinkage and densification. The rate at which the solvent can be removed is ultimately determined by the distribution of porosity in the gel. The ultimate microstructure of the final component will be strongly influenced by changes imposed upon the structural template during this phase of processing.

Afterward, a thermal treatment, or firing process, is often necessary to favor further poly-condensation and enhance mechanical properties and structural stability via final sintering, densification, and grain growth. One of the distinct advantages of using this methodology as opposed to the more traditional processing techniques is that densification is often achieved at a much lower temperature. The precursor sol can be either deposited on a substrate to form a film (e.g., by dip-coating or spin coating), cast into a suitable container with the desired shape (e.g., to obtain monolithic ceramics, glasses, fibers, membranes, aerogels), or used to synthesize

powders. The sol–gel approach is a cheap and low-temperature technique that allows fine control of the product's chemical composition. Even small quantities of dopants, such as organic dyes and rare-earth elements, can be introduced into the sol and end up uniformly dispersed in the final product. It can be used in ceramics processing and manufacturing as an investment casting material or as a means of producing very thin films of metal oxides for various purposes. Sol–gel derived materials have diverse applications in optics, electronics, energy, space, (bio)sensors, medicine (e.g., controlled drug release), reactive material, and separation (e.g., chromatography) technology. The detailing of this synthesis route is explained by the schematic block diagram below:

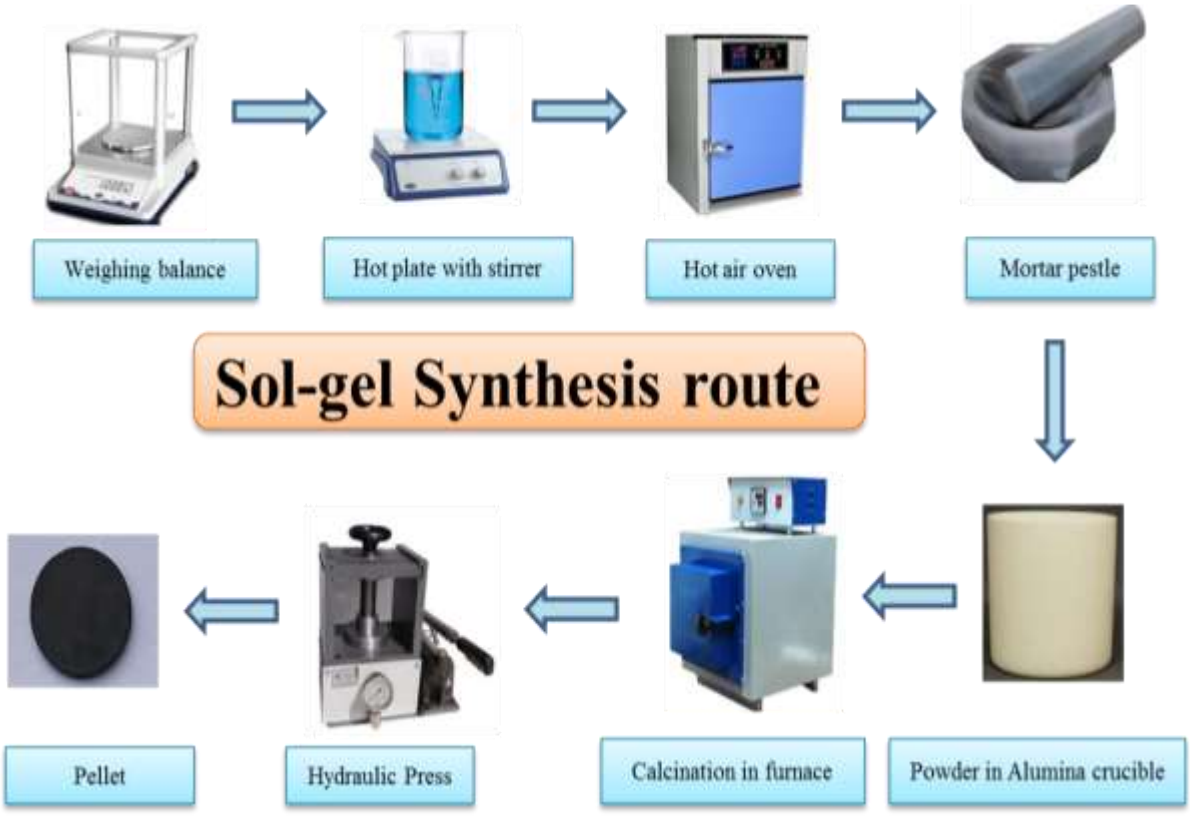

Figure 2.1 Schematic representations Sol-Gel Synthesis route

2.2.2 Solid-state reaction synthesis route

The solid-state reaction route is the most commonly used method to synthesize ceramic materials. First constituent oxides and/or carbonates are weighed according to their stoichiometric ratio in the chemical reaction equation used. After mixing very well, long hours of wet grinding are done in a high-quality mortar pestle to get a homogeneous powder. Acetone can be used as a medium during grinding. This homogeneously mixed powder is calcined in an alumina crucible at a higher temperature. During the calcination process, thermal decomposition, phase transition, or removal of a volatile fraction happens. This process usually takes place at temperatures below the melting point of the product materials.

In this heat treatment, the desired phase formation is due to various factors, such as solid-state diffusion of atoms, calcination temperature, and holding time. The detailing of this synthesis route is explained by the schematic block diagram below-

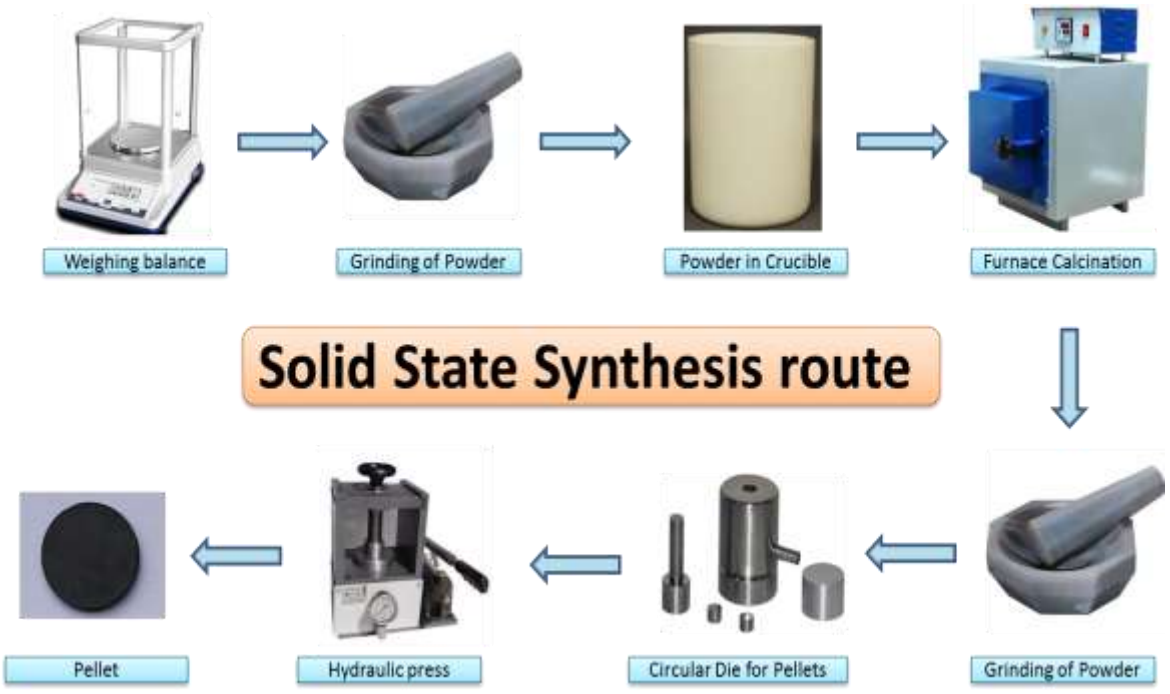

Figure 2.2 Schematic representations Solid State Synthesis Route

2.2.3 Pelletisation

For conductivity measurement, the powder was made into pellets of the required size and diameter by pressing it with a 7−8 ton weight on a hydraulic press. These pellets were made with the help of a press and die. Obtained pellets were fired at the required temperature for densification. The steps involved are shown in Figure 2.3.

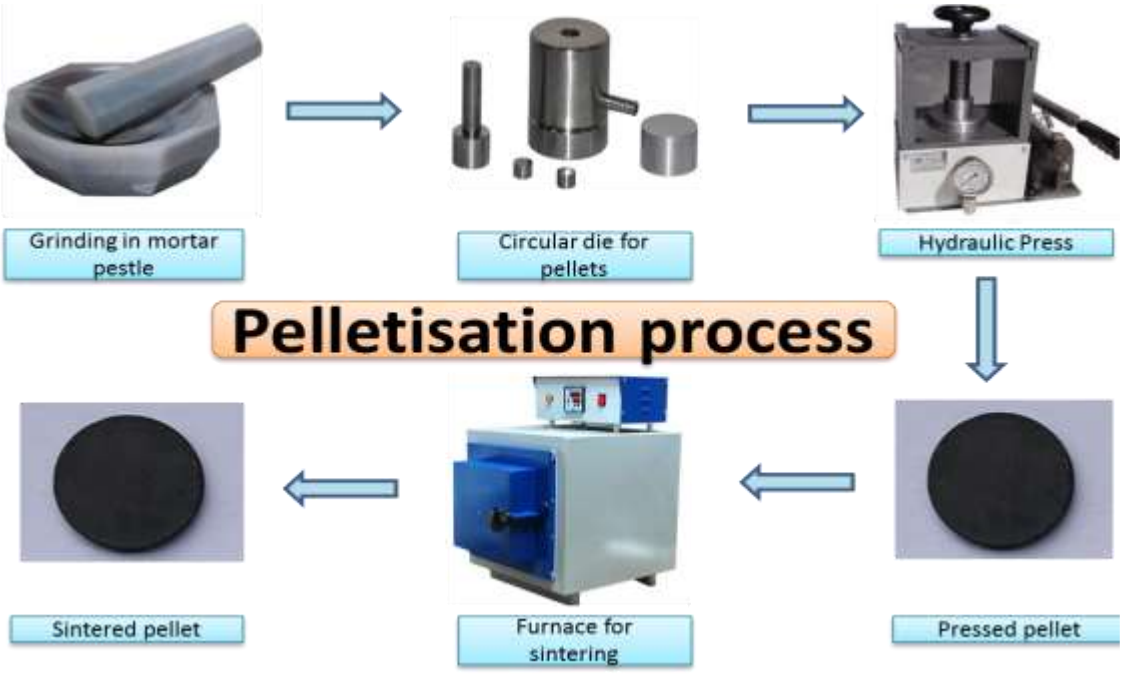

Figure 2.3 Schematic representations Pelletisation Steps

2.3 Material Characterization Techniques

The following section describes the characterization techniques used during this work. The basics of each method are briefly described in the next section. Here are the main techniques listed

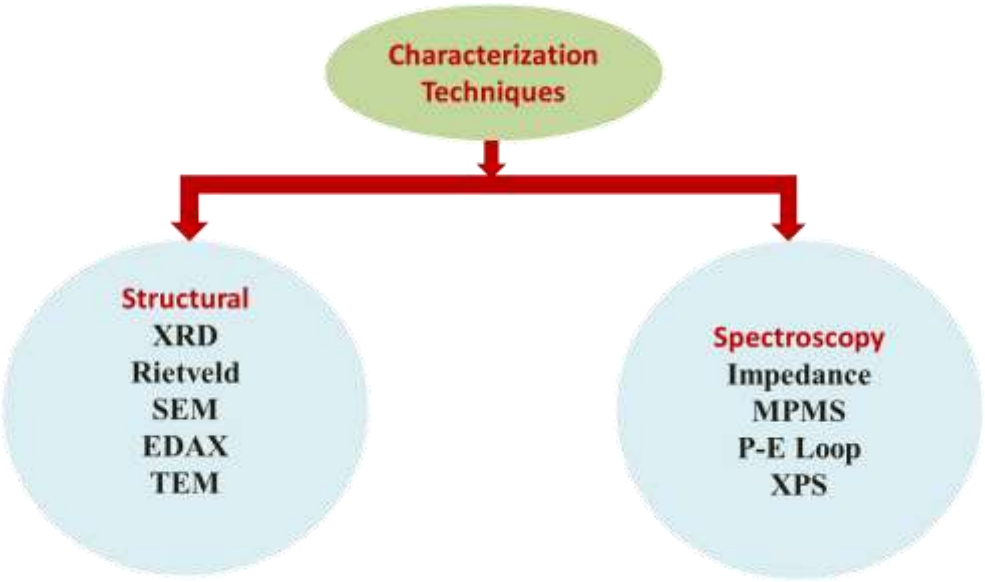

Figure 2.4 Characterization techniques used

2.3.1 Powder X-Ray Diffraction (XRD)

X-ray diffraction is an (XRD) powerful non-contact and non-destructive technique, making it ideal for structural studies. It identifies the crystalline phases present in the material. It can measure the structural properties like phase composition, grain size, preferred orientation, strain state, defect structure, and epitaxy of these phases present in the compound. The intensities obtained from the XRD can provide quantitative and accurate information on the atomic arrangements at interfaces. Materials having a different composition of elements can be successfully identified with XRD. Still, they are very sensitive to the elements having large atomic numbers because the diffracted intensities are enormous compared to those with lower atomic numbers. It predicts the quantitative phase analysis and qualitative structural and microstructural analysis.

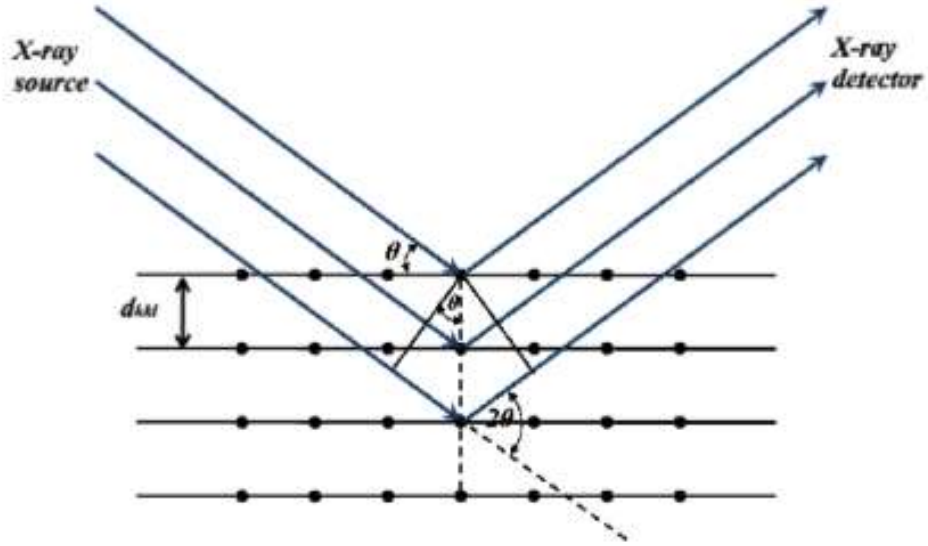

Figure 2.5 Demonstration for Bragg's Law

The diffraction satisfies the Bragg equation:

$$2dsin\theta = n\lambda \qquad (2.1)$$

Here d is the spacing between diffracting planes, is the incident angle, n is an integer, and λ is the beam's wavelength. [1-2]

The X–ray is generated in a Cu X–ray tube, filtered by a monochromator to increase sensitivity, collimated to concentrate, and directed toward the sample. The X–ray is diffracted by the atomic layers of the crystal, and the diffraction pattern is used for the analysis based on Bragg's diffraction law (nλ=2d sinθ). The 2θ positions of the diffraction peaks provide a fingerprint of the phases present and the intensity and spread of the peaks are used to obtain the quantity of each phase. The different phases were interpreted by recording an X-Ray diffraction pattern at room temperature on an X-Ray diffractometer (Rigaku Miniflex II, Japan) has Cu Kα radiation having wavelength λ= 1.5418 Å at an applied voltage of 40 kV and current of 40 mA. In this work, the XRD pattern has been recorded in the range of 20°-80° with a step size of 0.02.

2.3.2 Phase Confirmation and Crystal Structure Studies by Powder X-Ray diffraction

X-ray diffraction (XRD) is a versatile, non-destructive technique that reveals detailed information about the crystallographic structure of natural and manufactured materials. X-ray radiations most commonly used are that emitted by copper, whose characteristic wavelength for the Cu-K_α radiation is λ=1.5418Å. When the incident beam strikes a powder sample, diffraction occurs in every possible orientation of 2θ. The diffracted beam may be detected using a hybrid pixel array detector. Routinely, the 2θ range of 20 to 80 degrees is sufficient to cover the most valuable part of the powder pattern. The scanning speed of the counter is usually 2θ of 2° min^{-1}; therefore, about 30 minutes are needed to obtain a trace. Based on the principle of X-ray diffraction, a wealth of structural, physical, and chemical information about the material investigated can be obtained. A host of application techniques for various material classes are available, revealing the specific details of the sample studied.

Whether the unknown sample is single-phased or multi-phased, phase identification is the most crucial application of X-ray diffraction studies. This identification guides us in understanding the sources of mechanisms that are taking place behind this phase formation. This also gives an idea of the correlation of crystal structure with different properties, i.e. structure-property correlation (Neumann's principle).[2]

2.3.3 Rietveld Refinement

The sintered powdered samples were measured in an XRD instrument (Rigaku Miniflex II, Japan). The samples were exposed to a copper target and recorded at a range of 2θ = 20° – 80° with a scanning rate of 2°/min at a step of 0.02. The recorded

data were analyzed with Rietveld refinement "FullProf" software. Rietveld method uses the non-linear least square method and the measured data is compared with standard crystallographic database.

2.3.4 Scanning Electron Microscopy (SEM):

The scanning electron microscope (SEM) uses a focused beam of high-energy electrons to generate a variety of signals at the surface of solid specimens. The signals that derive from electron-sample interactions reveal information about the sample including external morphology (texture), chemical composition, and crystalline structure and orientation of materials. Data are collected over a selected area of the surface of the sample, and a 2- dimensional image is generated that displays spatial variations in these properties.

2.3.5 Fundamental Principles of Scanning Electron Microscopy (SEM):

Accelerated electrons in an SEM carry significant amounts of kinetic energy, and this energy is dissipated as a variety of signals produced by electron-sample interactions when the incident electrons are decelerated in the solid sample. These signals include secondary electrons (that produce SEM images), backscattered electrons (BSE), and diffracted backscattered electrons (EBSD that are used to determine crystal structures and orientations of minerals.[3]

2.3.6 Scanning Electron Microscopy (SEM) Instrumentation:

Essential components of all SEMs include the following:

- Electron Source ("Gun")
- Electron Lenses
- Sample Stage
- Detectors for all signals of interest
- Display / Data output devices

- Infrastructure Requirements:
- Power Supply
- Vacuum System
- Cooling system
- Vibration-free floor
- Room free of ambient magnetic and electric fields

SEMs always have at least one detector (usually a secondary electron detector), and most have additional detectors. The specific capabilities of a particular instrument are critically dependent on which detectors it accommodates.

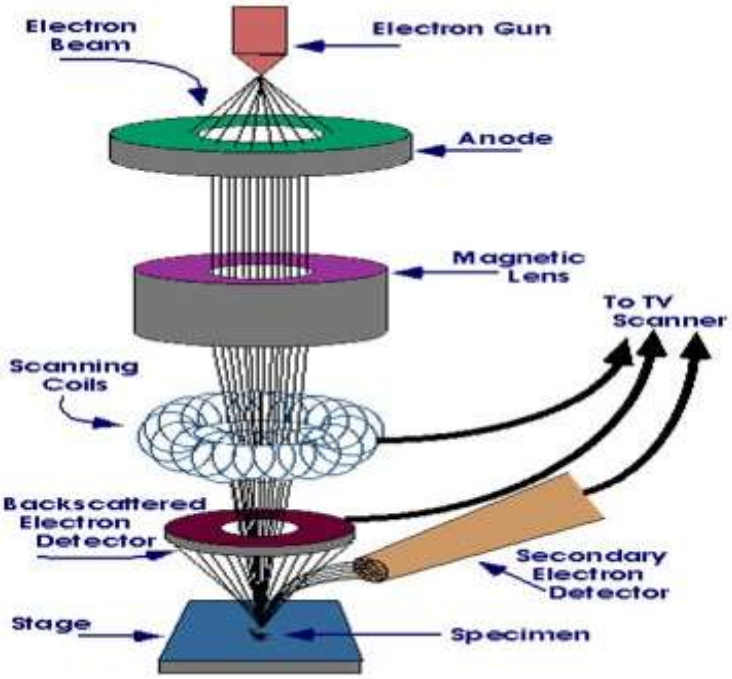

Figure 2.6 Schematic diagram of SEM

2.3.7 Energy Dispersive X-Ray Spectroscopy (EDAX)

The Energy Dispersive X-Ray analysis is a non-destructive X-ray analysis to identify the elemental composition of materials. This is generally attached with structural analysis techniques such as SEM and TEM, where a high-energy electron beam & the ejected electrons from the inner shell of an atomic orbital are used to

identify the specimen of interest. The resulting inner shell vacancy is filled by electrons available in the shell close to the vacant shell; these transitions are emitted as X-rays. Thus the information corresponding to the elements of the samples can be analysed based on the energy of emitted X-Rays. Sometimes X-Ray mapping may not show the distribution of elements that are not of interest because characteristics X-Rays of elements of interest are close to those not desired. It happens when the energy difference between the desired and undesired elements is equal to the spectrometer energy resolution. This method quantitatively evaluates the points on the sample while scanning the electron beam; that is why it is also called quantitative mapping of the sample. In this thesis work, we have used EDAX with HRSEM and HRTEM to study the electron mapping of the composition. [4]

2.3.8 Electrochemical Impedance Spectroscopy (EIS):

Electrochemical Impedance spectroscopy is a non-destructive technique & involves measurements and analysis of materials in which ionic conduction predominates. This technique is used in material research and development because it involves relatively simple electrical measurements, which can be readily automated. The results may often be correlated with many complex material properties. AC impedance used for SOFC material testing mainly provides information about oxide-ion conduction. It involves passing an AC voltage across a sample and measuring the resulting current response. Most of the materials have some degree of resistance and some capacitance. [5] They can be modeled as a series with resistance and capacitance. The current in the case of pure capacitive resistance can be shown in Equation (2.2)

$$i = \frac{E}{X_c} sin\left(\omega t + \frac{\pi}{2}\right) \qquad (2.2)$$

Where $X_c = 1/\omega_C$

$E = E_R + E_C$

Current for pure resistor can be shown as in Equation (2.3)

$$i = \frac{E}{R}\sin(\omega t) \qquad (2.3)$$

This data obtained through EIS is expressed in a Nyquist plot, where the imaginary part of the impedance (Z'') is plotted against the real part of the impedance (Z') as a function of frequency (ω). [6] An example Nyquist plot can be seen in Figure 2.13.

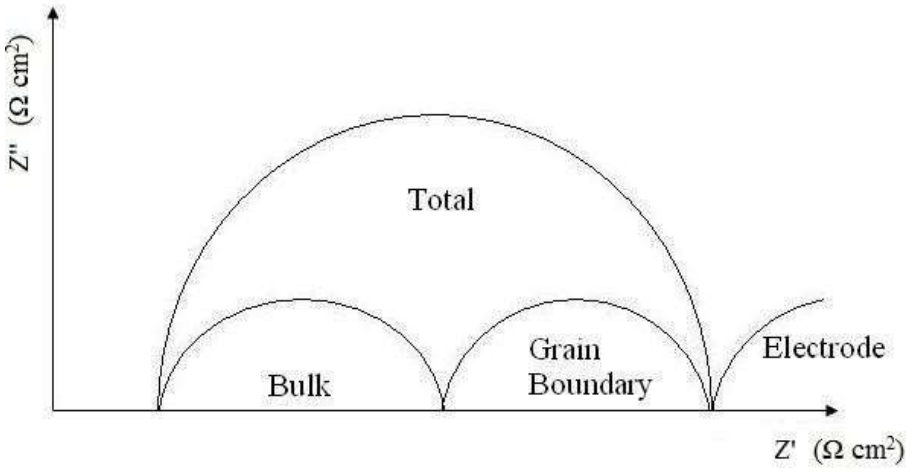

Figure 2.7 Nyquist Plot for ionic solids (Z'' = imaginary impedance, Z' = real impedance)

Numerous physical phenomena cause capacitance values of varying amounts, which can be easily identified on a Nyquist plot. For example, ionic resistance in the bulk of the material would have a capacitance value in the region of 10^{-12} F, whereas that of the grain boundaries within the material would have a capacitance value of 10^{-11} - 10^{-8} F. The bulk and grain boundary resistances can manifest themselves as separate curves on the Nyquist plot; however, it is not uncommon for the curves to be

partially or fully merged, especially when the resistance is significantly greater than that of the other. If impedance spectra are collected over a range of temperatures, it is possible to calculate the activation energy as per Equation 2.4.

$$\sigma T = Ae^{\frac{-E_a}{RT}} \quad (2.4)$$

Where σ = conductivity, T = temperature, A = sample surface area, E_a = activation energy and R = resistance

The Plot has been drawn between Log_{10} (σT)/S-$cm^{-1}K$ vs T^{-1} / K^{-1} to determine the activation energy, which is represented by the slope of the resultant line. [5-6]

2.3.9 Dielectric Measurement Using EIS

Our setup for measuring the dielectric is shown in Figure 2.8. It consisted of a sample holder which was set inside a split furnace The sintered pellets were coated with silver paste and cured at 500 °C for 30 min. The dielectric measurements were performed using an Autolab potentiostat as a function of frequency from 1 MHz to 1 Hz at different temperatures. All measurements were taken during the cooling cycle.

The impedance spectroscopy was carried out at a variable temperature in the air to study the dielectric behavior of the material. The dielectric constant was calculated using the formula:

$$\varepsilon_r = \frac{C*d}{\varepsilon_\circ * A} \quad (2.5)$$

Where; ε_r is the dielectric constant, C is capacitance, ε_o is the permittivity of free space ($8.85*10^{-12}$) F/m, d is the thickness of the pellet, A is the area of the pellet;

Capacitance (C) was calculated by using the formula

$$C = -\frac{1}{\omega}\left[\frac{Z''}{Z'^2 + Z''^2}\right] \qquad (2.6)$$

and the dielectric loss was calculated by

$$\tan\delta = \frac{\varepsilon''}{\varepsilon'} = \frac{Z'}{-Z''} \qquad (2.7)$$

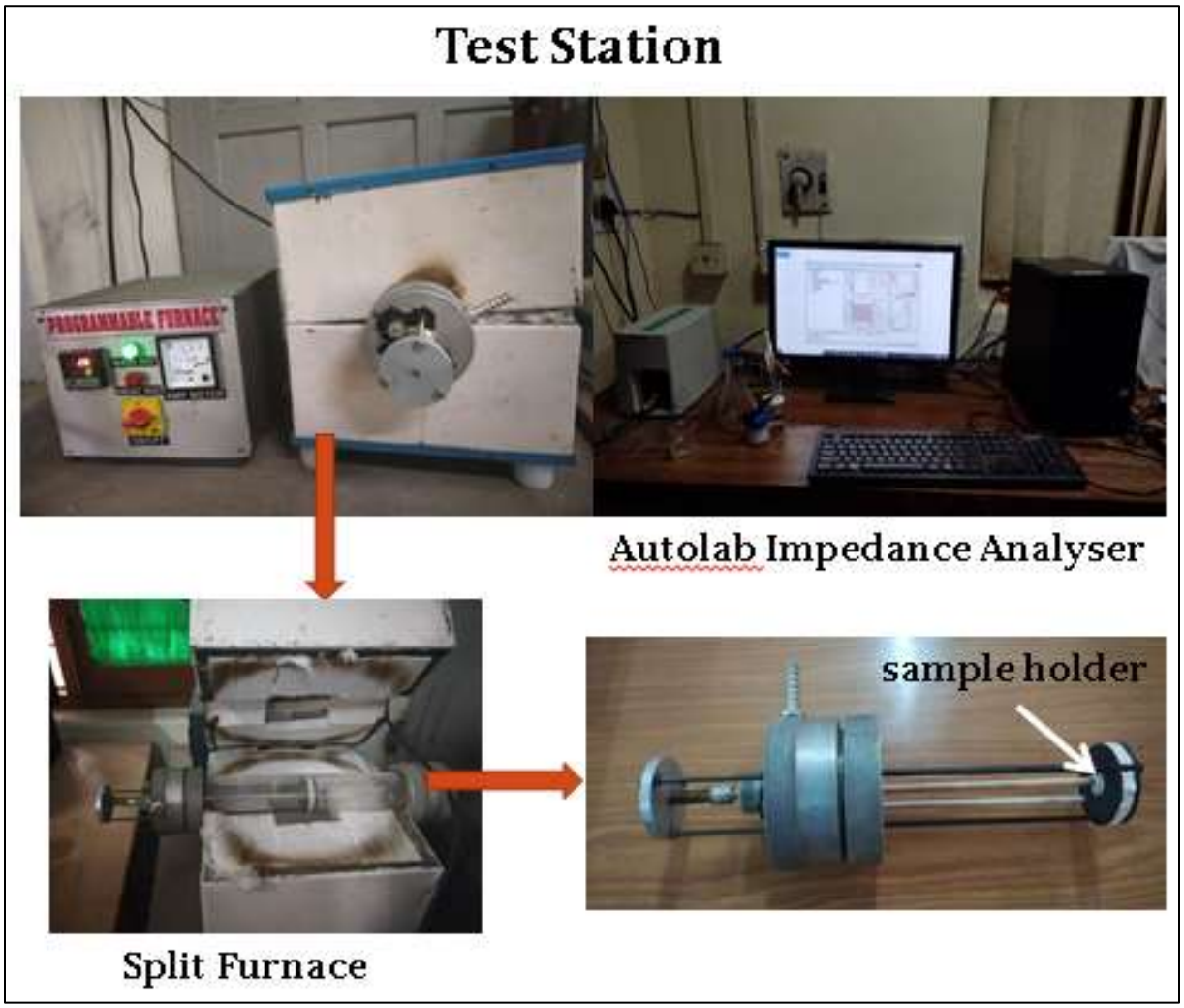

Figure 2.8 Schematic representations Dielectric Test station

2.3.10 Magnetic Measurement

Magnetic measurement is performed with the superconducting quantum interference device (SQUID). It is a highly sensitive flux-meter, which measures the magnetic behavior of the samples when subjected to different temperatures, pressures,

and changes in the magnetic field. In SQUID, a vacuum is created by liquid helium, and the temperature inside the chamber is maintained with liquid nitrogen. The sensitivity of the instrument is highly maintained by holding the magnetic field constant by a superconducting shield. The sample of a specific size (2mm×2mm×4mm), fixed with a varnish in a tufnol holder positioned at the end of a carbon rod between the two pick-up coils, the sample moved slowly through the pickup coils, and the quanta are counted.

Then the magnetic field is applied it moved through the coil in a series of 32 steps. To convert the signal into an electromagnetic unit (emu), the sample is moved to a fixed distance of 4 cm and the generated signal is measured. A schematic diagram of SQUID is shown in Figure 2.9

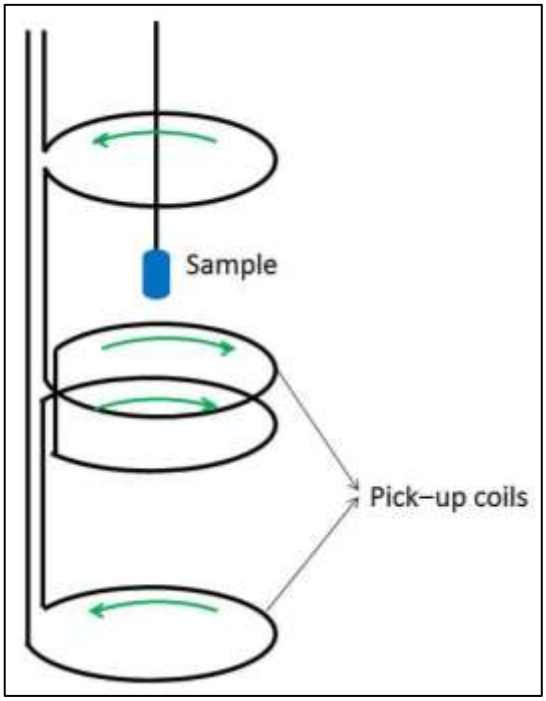

Figure 2.9 Working principles of MPMS.

In this thesis work SQUID magnetometer of Quantum design, Model–MPMS 3, EM–QM, USA was used. It has a range of field ±7T (tesla).

2.3.11 Ferroelectric Measurement

It is a measurement system to prove the ferroelectricity by reversal of spontaneous polarization on the application of an electric field.

Poling: The purpose of poling is to make a material anisotropic by applying an external electric field which tends to have domains aligned in the same direction as the field and the removal of the field leaves a net remnant polarization.

In this thesis work the sintered pellets of thickness ~1mm were silver coated on both sides and then polled at room temperature by placing the pellets in the silicon oil with a DC poling unit (Marine India).

The polarization (P)

$$P = \frac{V_c}{a} - \varepsilon_0 E \qquad (2.8)$$

Here, V_c is the voltage of the constant capacitor, a is the area of the coated surface.

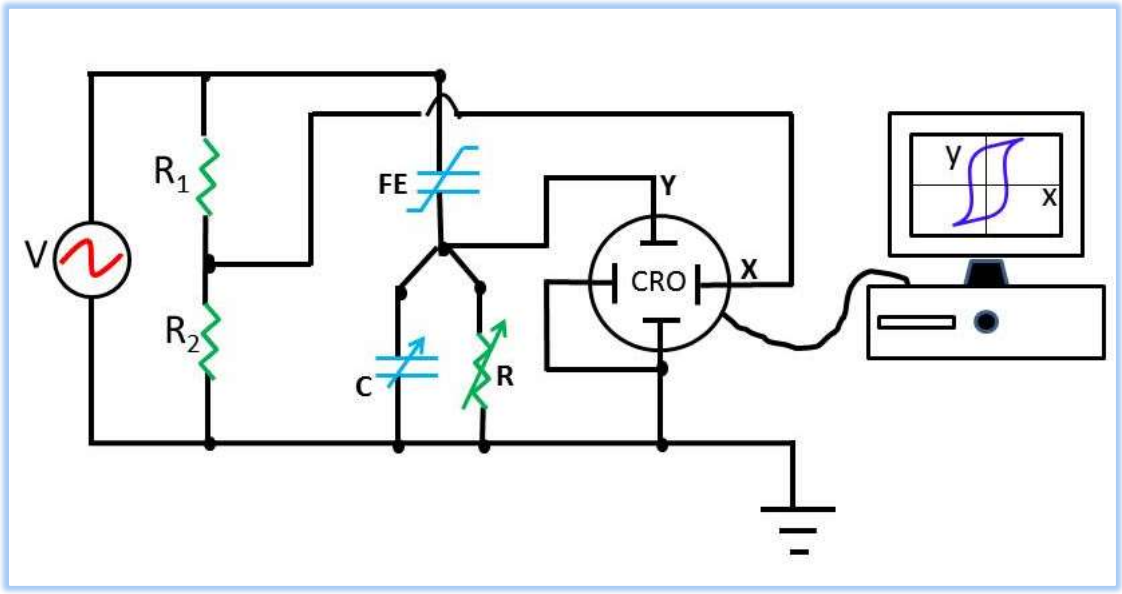

Figure 2.10 Sawyer-Tower electric circuit diagrams for ferroelectric hysteresis loop measurement.[7]

2.3.12 X-ray photoelectron spectroscopy

X-ray photoelectric absorption is based on the photoelectric effect (ejection of electrons from a material when electromagnetic radiation strikes its surface). In this technique x-ray beam is irradiated on the sample surface and the ejected electrons provide the information of present elements. XPS study was also applied for line profiling of elemental composition. XPS requires ultra-high vacuum ($p < 10^{-7}$ Pa) conditions. XPS can detect all elements except hydrogen and helium. The detection limit is in the parts per thousand range, but parts per million (ppm) are achievable with long collection times and concentration at the top surface.

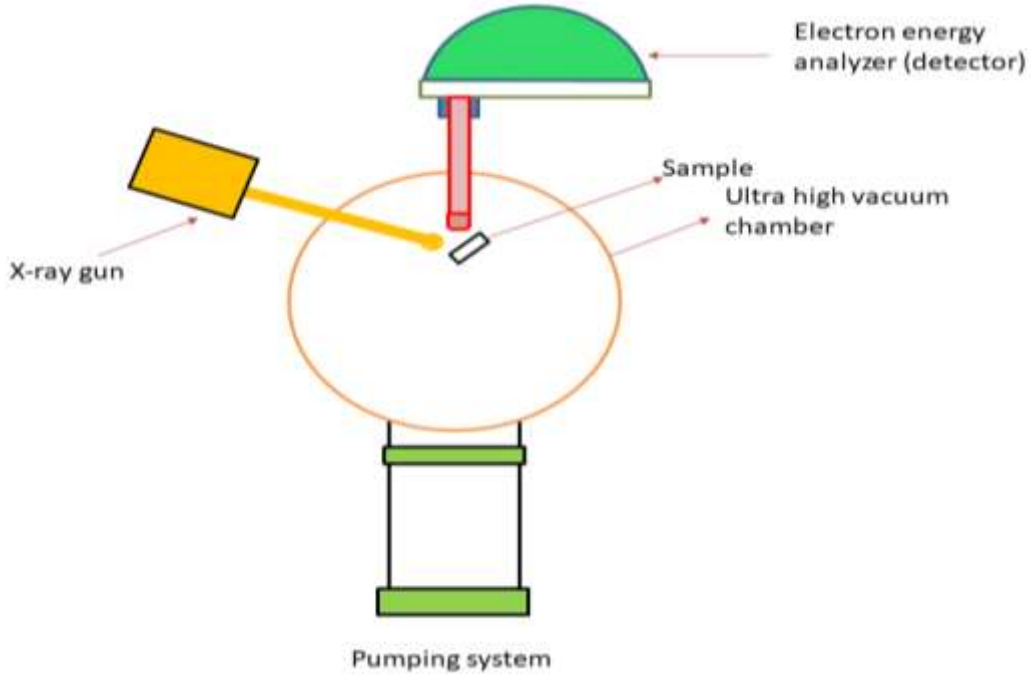

Figure 2.11 Systematic diagrams of XPS

XPS is routinely used to analyze inorganic compounds, semiconductors, metal alloys, polymers, glasses, ceramics, paints, papers, inks, woods, plant parts, bio-materials, viscous oils, glues, ion-modified materials, hydrated forms of materials (hydrogels) and many others.

References

1. Borie, B. X-Ray Diffraction in Crystals, Imperfect Crystals, and Amorphous Bodies. Journal of the American Chemical Society. 1965, pp 140–141.
2. B. D Cullity, Elements of X- Ray Diffraction.
3. W. C. Nixon Phil. Trans. Ray. Soc. Lond.B.261, 45-50 (1971)
4. https://en.wikipedia.org/wiki/Energy-dispersive_X-ray_spectroscopy
5. Anthony R. West Solid State Chemistry and its Applications, 2nd Edition, March 2014
6. Thomas William Pike, PhD thesis on Development & processing of Solid Oxide Fuel Cell Materials, University of Birmingham.
7. Yuewei Yin, Ferroelectric measurement, 2016/01/29.